



Comparing Adsorption Properties of Algerian Kaolinite Towards Phosphate with Those of Activated Carbon: Adsorption Experiments, Molecular Modeling and an Initiative Toward Hydroponic Wastewaters Remediation

Meriem Fizir · Amina Richa · Sami Touil · Rachid Fermous ·
Chahinez Tahir · Imane Hassene · Liu Wei · Houda Douba

Received: 30 March 2023 / Accepted: 1 June 2024 / Published online: 12 June 2024
© The Author(s), under exclusive licence to Springer Nature Switzerland AG 2024

Abstract In this research, adsorption properties of an Algerian kaolinite (KNTs) for removal of phosphate from aqueous solutions was compared with those of a commercial activated carbon (AC) in term of kinetics, equilibrium, and thermodynamic studies. Fourier Transform Infrared (FTIR) spectroscopy and X-ray diffraction (XRD) was used to characterize the adsorbants. Effect of various reaction parameters such as pH, adsorbent dose, adsorption time, and temperature on PO_4^{3-} adsorption by both adsorbents were explored and compared. Adsorption experiments showed that KNTs is a good adsorbent of phosphate. However, it is not superior to AC in terms of adsorption capacity. The maximum uptake capacity of AC and KNTs (71.89 and 16.93 mg/g) have been reached after 60 and 250 min, respectively. The two adsorbents showed a higher phosphate removal rate of 93.74% for AC and 69% for

KNTs. The pH of the solutions, affect considerably the adsorption mechanism. The removal capacity results of PO_4^{3-} by KNTs showed significant fit with both pseudo-first-order and pseudo-second-order models proving the dominance of both physisorption and chemisorption mechanisms during the uptake of phosphate. Whereas, the adsorption of PO_4^{3-} by AC found to be controlled by physisorption only. Isotherm simulation studies of the adsorbents showed that KNTs presented high heterogeneity degree than AC and the adsorption of phosphate is well described by Temkin model. Adsorption/desorption experiments suggested that KNTs could be successfully regenerated in multiple times (at least three). Based on theoretical calculations, different configurations of KNTs@PO_4^{3-} were obtained after minimizing their energy using MM2 Server. The later revealed that phosphate with more charged (HPO_4^{2-}), showed greater interaction energy than

Supplementary Information The online version contains supplementary material available at <https://doi.org/10.1007/s11270-024-07235-w>.

M. Fizir (✉) · A. Richa · S. Touil
Laboratory of Precision Agriculture, Environment
and Sustainable Development, Khemis Miliana University,
Khemis Miliana, Algeria
e-mail: meriem.fizir@univ-dbk.m.dz

M. Fizir · R. Fermous · C. Tahir · I. Hassene · H. Douba
Laboratoire de Valorisation Des Substances Naturelles,
Khemis Miliana University, 44225 Khemis Miliana,
Algeria

L. Wei
Zhejiang Pharmaceutical University, Ningbo, 315500,
Zhejiang, China

H. Douba
Laboratory Physical Chemistry of Materials Interfaces
Applied to the Environment, University of Saad, Dahlab
Blida1, 09 000, Blida, Algeria

H_2PO_4^- , which indicated that HPO_4^{2-} interaction with KNTs are more stable. The adsorption experiments in real hydroponic wastewaters further indicated the application potential of KNTs. This research offered potential candidate (Algerian kaolinite) for water cleaning up against phosphate contamination.

Keywords Adsorption · Kaolinite · Activated carbon · Phosphate

1 Introduction

Designated in chemistry by the letter P, phosphorus is a vital element present in all living organisms (Kong et al., 2023) and it is one of the main growth-limiting nutrients for crops (Peng et al., 2022; Tao et al., 2022). The worldwide utilization of fertilizer based phosphate is increasing due to elevated-input modern agricultural activities (Zheng et al., 2023). For example, cultivation of crops with hydroponic methods or soilless cultivation system is almost in 100% carried-out in open fertilization systems, from where the surplus of nutrient solution is released in an uncontrolled mode to the surface water (Hosseinzadeh et al., 2017, 2019). Typically, large quantity of wastewater containing high phosphorus (15–100 mg $\text{PO}_4\text{-P/L}$) and other elements such as nitrates (Gagnon et al., 2010; Park et al., 2015; Richa et al., 2020) could be generated from hydroponic system. The well-known source of water quality deterioration is the excessive phosphate discharge from hydroponic wastewaters which may lead to the eutrophication ($> 30 \mu\text{g PO}_4^{3-}\text{-P/L}$) that generates aquatic plant bloom and the related depletion of dissolved oxygen, and that severely alters the quality of water (Nie et al., 2023). In another hand, the danger of phosphate effects human health as it is the origin of liver and kidney failure in addition to damage to the intestines, and bones (Eltaweil et al., 2023). Thus, World Health Organization stated that the suitable dosage of phosphate in drinking water should be less than 5 mg/L (Isiuku & Enyoh, 2020; Kong et al., 2019). Consequently, elimination of excess phosphate from water is necessary.

In another hand, the good quality mineable rock phosphate (mineral P) supply is in the way to get exhausted in 100 years if the consumption rate continues (Li et al., 2023; Peng et al., 2022; Yang et al.,

2023). Accordingly, finding alternate sources of phosphorus or find a feasible technique to recover it from wastewaters is urgently needed and the sustainability will be enhanced by its exploitation in agriculture (creation a cyclic process).

There are many publications dealing with phosphate remediation from aqueous system where plentiful technologies have been developed for aqueous phosphate removals which include chemical precipitation (Haiming Huang et al., 2017a, b), biological method (Zhang et al., 2023), reverse osmosis (Seminskaya et al., 2017), electrochemical methods (Ren et al., 2022), crystallization (Xuechu et al., 2009), constructed wetlands (Park et al., 2017), nanofiltration (Loh et al., 2022), and ion exchange (Ali et al., 2022). These technologies showed high efficiency even at low phosphate concentration and generate no waste. However, it suffers from serious drawbacks. For example, high infrastructural investment and highly skilled personal is required in biological methods (Owodunni et al., 2023). Nanofiltration, ion exchange and reverse osmosis have a high operational and maintenance cost (Zhang et al., 2022). Electrocoagulation required high capital cost and skilled labor as well (Hu et al., 2022). Constructed wetland process need larger land areas (Konadu-Amoah et al., 2022). It is widely recognized the most efficient methods for phosphate removal with advantages of low-cost, high efficiency (a wide range of concentration), and simple operation (Manna et al., 2022) is adsorption. Recovering phosphate for use in agriculture is a feasible strategy that can be attained by adsorption process. Different adsorbents with unique sorption characteristics and surface regeneration-capacities have been examined. Activated carbon (AC) (Ouakouak & Youcef, 2016; Shao et al., 2022), carbon nanotubes (Liu et al., 2022) and graphene oxide (Lee et al., 2020) as single materials or anchored with polymers such as chitosan, or alginate (Eltaweil et al., 2023) are commonly used due to their high efficiency and large surface area; however, they have a higher cost relative to other adsorbents (Fizir et al., 2022a, b). In addition, researchers now are committed to find an efficient, economic and simple adsorbent instead of complicated adsorbents that contain different materials.

More recently, the development of an economic adsorbents such as kaolinite (KNTs) and halloysite nanotubes (HNTs) due to their relative abundance,

environmental compatibility, and adsorption efficiency have been gaining attention for aqueous inorganic pollutants removal (Almasri et al., 2019; Kamiyango et al., 2009; Kumar & Viswanathan, 2020; Zheng et al., 2023). Kaolinite is a hydrous aluminum phyllosilicate member belonging to the dioctahedral 1:1, kaolin mineral group (Awad et al., 2017). Kaolinite usually shows platy morphology, the basic plane of oxygen atoms in a crystal unit is confronted with the basal plane consisting of OH ions in the next layer (Murray, 2006). Besides the biocompatibility and economic properties of KNTs, it possess high porosity, unique compositions (abundant hydroxyl groups on the surface), and large specific surface area that allow them to interact with a variety of organic and inorganic molecules (Mustapha et al., 2019, 2021). To date, the scientific literatures on the use of kaolin for the treatment of phosphate wastewater are very scarce compared to AC. In these studies, encouraging results were obtained since the maximum removal capacity (69.7%, ~ 0.8 mg/g) of phosphate from aqueous solution was obtained by using a high dose of Linthipe kaolinite (80 g/L) (Kamiyango et al., 2009). In another research, 2 g of kaolin clay showed removal capacity of 45.6% (0.46 mg/g) toward phosphate (Al-Zboon, 2018). These findings could be enhanced under optimum laboratory conditions. Consequently, the adsorption process and mechanism of phosphate on KNTs need to be explored more and optimum condition for phosphate removal along with kinetics; isotherm and thermodynamic behavior should be elaborated by using non linear regression analysis method instead of linear method as it is more reliable and suit better the adsorption process of various analytes. What's more, the practical application of KNTs in real wastewaters has not been reported anywhere. Thus, a comprehensive and detailed study of the phosphate removal capability of low-cost kaolin should be conducted to assess the applicability of this attractive nanomaterial in the treatment of phosphate contaminated wastewater such as hydroponic wastewaters in the future. The aim of this study was to evaluate for the first time the ability of Algerian kaolinite clay to remove phosphates from an aqueous solution and hydroponic wastewaters and to compare its adsorption capacity with commercial activated carbon. Moreover, the role of the kaolinite mineral in phosphate removal was carefully investigated through kinetic, isotherm, thermodynamic studies.

In addition, the adsorption mechanism of phosphate onto KNTs by molecular mechanical method (MM2) was explored for the first time through using Chem3D Pro which is software that provides computational tools based on molecular mechanics (MM) for optimizing models, conformational searching and molecular dynamics (Debbaudt et al., 2004; Huang et al., 2019; Jawla & Kumar, 2013; Yoo et al., 2023). The regeneration ability of KNTs has been examined as well.

2 Material and Method

2.1 Materials

Potassium dihydrogen phosphate (KH_2PO_4), hydrochloric acid (HCl), sodium hydroxide (NaOH), sulfuric acid (H_2SO_4), ammonium molybdate, Ascorbic acid and potassium antimonyl tartrate were obtained from Merck Chemicals (Darmstadt, Germany). KH_2PO_4 was dissolved in purified water to prepare a stock solution containing 1 g/L of PO_4^{3-} . Direct-Q 3UV purification system is used for water generation. Kaolinite was obtained from the Djebel Debbagh deposit located in the eastern region of Algeria. The preparation of KNTs involved following the method described by Zhao et al. (Zhao et al., 2011). In summary, the samples were dispersed in deionized water and filtered using a 53 μm (270 mesh) sieve to eliminate most of the sand particles. The clay fraction, consisting of particles with a diameter less than 2 μm , was separated using a sedimentation technique. Subsequently, the clay fraction was subjected to an acid wash to remove any impurities that could dissolve. The sample was then neutralized to restore its natural pH. Finally, the clay was dried and stored in plastic bottles for future use. Activated carbon was supplied from Sigma Aldrich. Hydroponic nutrient solution used to grow lettuce and discharged as wastewater was collected from a glasshouse operation at Khemis-Miliana University, Algeria. The analysis of composition and physical properties of wastewaters should be carried out before the batch experiments.

2.2 Determination of pH_{pzc} of Adsorbents

To investigate the adsorption mechanism of phosphate, point of zero charge (pH_{pzc}) values of the

studied adsorbents was estimated by salt addition process (Khan et al., 2019). Briefly, 0.5 g of KNTs or AC mixed with 20 mL of 0.01 M NaCl after regulating the pH of the solutions (from 2 to 10) with base or acid. The flasks were agitated for 24 h at 298 K and 160 rpm. Then, the final pH was measured in each flask after solution centrifugation process. The pH_{pzc} values of AC and KNTs were determined from the pH_{final} versus $pH_{initial}$ plot.

2.3 Characterization

Scanning electron microscopy (THERMOSCIENTIFIC QUATTRO S SEM) was employed to investigate the surface morphology of the KNTs. X-ray diffraction patterns for KNTs and AC were recorded in reflection mode in the angular range of $1-90^\circ$ (2 theta), at 298 K by a D8 Advance Eco (Bruker) operated at a $CuK\alpha$ wavelength of 1.542 \AA . FTIR analyses of the adsorbents were executed on a FTIR-8400 spectra scanner (SHIMADZU). The Brunauer–Emmett–Teller (BET) surface area of the KNTs and AC were obtained by nitrogen adsorption–desorption isotherms at 77 K using a specific analyzer (ASAP2020) and found to be $22.253 \text{ m}^2/\text{g}$ for KNTs and $1024 \text{ m}^2/\text{g}$ for AC (Table 1). The cation exchange capacity (CEC) of KNTs measured by Ba^{2+}/NH_4^+ exchange was $17 \text{ cmol}/\text{kg}$ (Zhao et al., 2011).

2.4 Batch-adsorption Experiments

The ability of the KNTs and AC in the removal of PO_4^{3-} has been examined using batch adsorption modes. To attain the ideal adsorption capacity, the primary parameters, including solution pH, adsorbent dose, temperature, contact time and initial phosphate concentration were preliminarily examined. Typically, the mixed PO_4^{3-} solution pHs were regulated using diluted base or acid solutions and

mixed with a determined quantity of each adsorbent (10 mg) in flasks containing 10 mL of a PO_4^{3-} solution. Subsequently, the mixed suspensions were agitated at 200 rpm at a predetermined temperature for a fixed contact time. Specific quantity of KNTs and AC were mixed with phosphate solutions at fixed initial concentrations and optimum pH values. After equilibrium, samples were centrifuged. The concentration of PO_4^{3-} in the supernatant was analyzed by spectrophotometer (Spectronquant prove 300) at a wavelength of 710 nm by ammonium molybdate spectrophotometry (Nagul et al., 2015). The adsorption capacity (mg/g) and the removal rate (%) of the adsorbents were measured using the following equations:

$$Q = (C_0 - C_e) * V / m \quad (1)$$

$$\text{Removal rate (\%)} = ((C_0 - C_e) / C_0) * 100 \quad (2)$$

where C_0 and C_e (mg/L) are the initial phosphate concentrations at equilibrium in the solutions, respectively. V is the volume (mL) of the aqueous solution. m is the quantity (g) of adsorbents.

For kinetic experiments, 10 mg of KNTs and AC were added to 10 mL of PO_4^{3-} solutions (100 mg/L), and the solution was shaken at 298 K for different reaction times (5 min to 6 h). The pseudo-first-order, pseudo-second-order, Elovich, and Weber Morris Intra-Particle Diffusion models were used to assess the adsorption kinetics of phosphate by KNTs and AC and determine the rate constant of the process. The nonlinear equation of each model is depicted in Table 2. For adsorption isotherm assessments, 10 mg of each adsorbent were suspended in PO_4^{3-} solution of various concentrations (30–306 PO_4^{3-} mg/L) at 298 K. Langmuir, Freundlich, and Temkin models were exploited to describe the adsorption equilibrium of phosphate by KNTs and AC. The nonlinear equations of these isotherm models are presented in Table 3. The above- experiment protocols were detailed in the Supporting information (SI).

2.5 Sorbent Regeneration Study

Stability and cost effectiveness are among the main characteristics of good adsorbent. To validate these

Table 1 BET surface area, pore volume and pore diameter of KNTs and AC

Samples	BET surface area (m^2/g)	Pore volume (cm^3/g)	Pore diameter (nm)
KNTs	22.253	0.122	23.730
AC	1024	0.572	2.23

features, regeneration study need to be examined (Fizir et al., 2018). Briefly, specific amount of KNTs and AC were utilized in 4 successive cycles of sorption/desorption in aqueous samples using optimum experimental conditions. For desorption tests, 10 mL of diluted NaOH (eluent, 0.1 M), was mixed with the used adsorbents for 2 h. Once desorption equilibrium was attained, the adsorbents were separated and the amount of desorbed phosphates was measured (Elta-weil et al., 2023; Patel, 2021).

2.6 Molecular Modeling Analysis

A molecular modeling investigation was implemented to discover and explore the adsorption characteristics of phosphate onto the KNTs. CHEM3D software (version 20.0, PerkinElmer, Waltham, MA, USA) was utilized to visualize 3D structure models of the diverse forms of phosphate and KNTs. The MM2 was employed as an energy minimization technique for geometry optimization of phosphate and KNTs.

Table 2 List of kinetic adsorption models (Teng & Hsieh, 1999; Wang & Guo, 2022)

Model	Non linear equation	Parameters
Pseudo-first-order (PFO)	$Q_t = Q_e [1 - \exp(-K_1 t)]$	Q_e and Q_t are the phosphate adsorption capacities (mg/g) at equilibrium and at time t , respectively k_1 (min^{-1}), k_2 (g/mg.min), and k_3 (mg/g.min ^{1/2}), are the rate constant of the first-order kinetic, second-order kinetic, and weber morris intra-particle diffusion models α (mg/g.min) is the initial adsorption rate β (g/(mg.min)) is the extent of surface coverage
Pseudo-second-order (PSO)	$Q_t = \frac{K_2 Q_e^2 t}{1 + Q_e k_2 t}$	
Elovich	$Q_t = \frac{1}{\beta} \ln(1 + \alpha \beta t)$	
Weber Morris Intra-Particle Diffusion	$Q_t = K_3 t^{1/2} + C$	

Table 3 List of isotherm adsorption models (Xu et al., 2020)

Model	Non linear equation	Parameters
Langmuir	$Q_e = \frac{K_L Q_{\max} C_e}{1 + K_L C_e}$	Q_e (mg/g) is the phosphate adsorption capacity C_e (mg/L) is the phosphate concentration in solution in equilibrium Q_{\max} (mg/g) is the Langmuir maximum adsorption capacity of the adsorbent K_L (L/mg) is a constant related to the energy of adsorption K_F (mg/g)/(mg/L) ⁿ is the Freundlich constant, and n (dimensionless) is the Freundlich intensity parameter K_T is the Temkin constant, respectively RT/b_i is related to the heat of biosorption
Freundlich	$Q_e = K_F C_e^{1/n}$	
Temkin	$Q_e = \frac{RT}{b_i} \ln(K_T C_e)$	

Fig. 1 SEM images of KNTs (A-B)

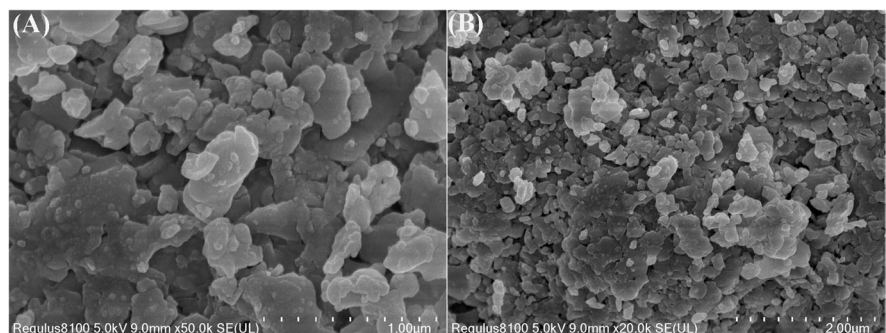


Fig. 2 The XRD patterns of KNTs and AC

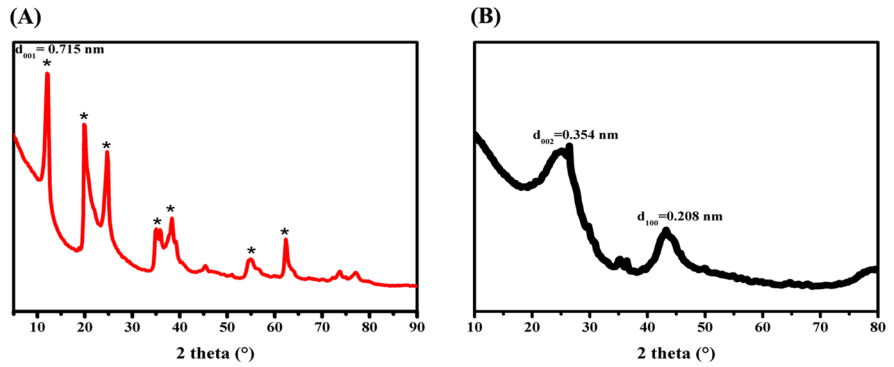


Table 4 Data of technical XRD kaolinite

Samples	interlayer spacing (nm)		
	d ₀₀₁	d ₀₀₂	d ₁₀₃
Pure Kaolinite	0.714	0.357	0.234
Algerian KNTs	0.715	0.357	0.234

3 Results and Discussion

3.1 Characterization

3.1.1 SEM Analysis

It can be observed from SEM images (Fig. 1) that KNTs consists of irregular crystals with uneven

fringes and the particle size of KNTs are generally in the sub-micron size range (< 1 μm). The SEM images of AC (Fig. S1), as analyzed in previous research (Alahabadi et al., 2017), show a porous structure with scattered holes and a smooth surface.

3.1.2 X-ray Diffraction

As shown in Fig. 2A, The absorption peaks found at 2 theta (°) = 12.36°, 20.43°, 21.42°, 24.86°, 35.90° and 38.46°. The maximum size of the crystallites appears at the absorption peak of 24.86°. The peaks of kaolinite were located at 2 theta angles values of 12.36° and 24.86°. The 2 theta diffraction angles for quartz are clearly visible at 26.6° (Dewi et al., 2018). Table 4 showed the interlayer spacing (d_{hkl}) of pure KNTs and

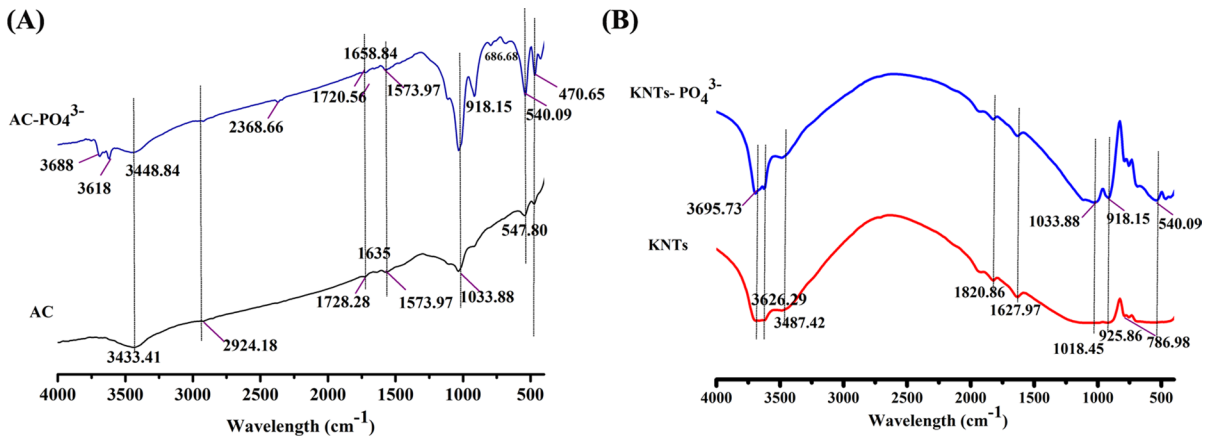


Fig. 3 FTIR spectrum of (A) AC and (B) KNTs before and after PO₄³⁻ adsorption

Algerian KNTs used in this study calculated using Bragg's equation. The data shows the value of commercial kaolin $d(\text{\AA})$ used in our study and the pure kaolin has no difference.

The diffraction pattern of the activated carbon used (Fig. 2B) shows its amorphous nature. It is characterized by the presence of the two broad bands ($2\theta = 26^\circ$ and 43°) observed in several studies, which are respectively related to (002) and (100) the diffraction peaks of the graphitic pore walls (Alahabadi et al., 2017).

3.1.3 FTIR Analysis

The FTIR spectrum of the AC (Fig. 3A) revealed several absorption bands indicating the presence of specific functional groups. The absorption band at 3433 cm^{-1} corresponds to the stretching vibrations of OH groups in phenolic groups (Biniak et al., 1997). The bands at 1635 cm^{-1} are attributed to the bending vibrations of O–H bonds in hydroxyl functional groups or chemisorbed water. The band at approximately 2920 cm^{-1} identifies stretching vibrations of aliphatics groups ($-\text{CH}_2-$). The bands at around 1500 and 1750 cm^{-1} can be attributed to axial C=O strain, such as highly conjugated C=O stretching or C–O stretching in carboxyl groups, respectively. The band observed at 1033 cm^{-1} corresponds to the elongation of C–O bonds in ethers and esters (Fan et al., 2016; Shu et al., 2017). The shift in the peak belonging to OH from 1635 cm^{-1} to 1658 cm^{-1} suggests

the involvement of OH groups in the adsorption of phosphate. In addition, in the FTIR spectrum of AC adsorbed with phosphate ions shows several absorption bands, including those at 540 , 686 , 918 , 1033 cm^{-1} , which are characteristic of PO_4^{3-} groups. Moreover, most of the significant FTIR bands of AC were preserved and shifted in wavenumber, confirming the adsorption of PO_4^{3-} (Elmsellem et al., 2013).

As shown in Fig. 3B, KNTs functional groups for the Si–O stretching vibration are visible at 1018 cm^{-1} . The peak at 786 cm^{-1} can be attributed to the stretching vibration of Si–O–Al. Additionally, peaks at 925 and 3695 cm^{-1} can be assigned to the Al–OH stretching vibrations of the alumina sheets in the kaolinite (Ge et al., 2019). In the FTIR spectrum of KNTs adsorbed by PO_4^{3-} , the FTIR bands of KNTs were preserved, but they shifted in wavenumber, indicating the adsorption of phosphate ions. For instance, the characteristic peak of Al–OH shifted slightly from 925 cm^{-1} to 918 cm^{-1} , which suggests the affinity of aluminum to phosphate ions. Furthermore, the asymmetric stretching and bending modes of PO_4^{3-} at 1033 cm^{-1} and 540 cm^{-1} in KNTs- PO_4^{3-} confirm the adsorption of phosphate ions (Kumar & Viswanathan, 2020).

3.2 Effect of Solution pH

The results in Fig. 4A revealed that PO_4^{3-} adsorption by KNTs and AC is pH dependent and the adsorbed quantities of the PO_4^{3-} on the KNTs and AC are

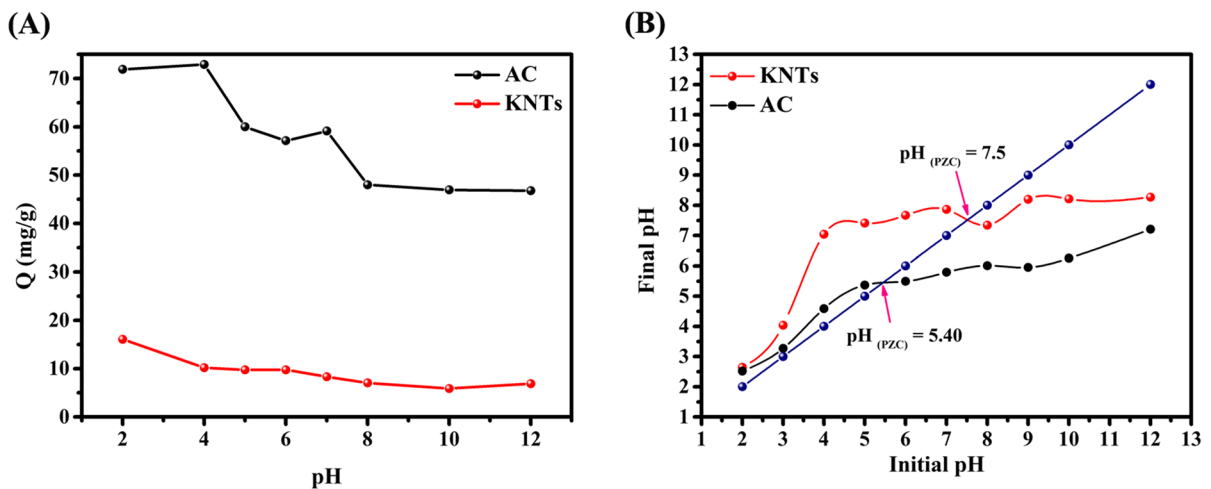


Fig. 4 (A) Effect of pH for phosphate adsorption and (B) Point of zero charge analysis of KNTs and AC

higher at pH 2 and 2–4, respectively. For example, the quantity adsorbed is reduced sharply from 16.93 mg per g of KNTs to 6.88 mg per g of KNTs for pH 2 to 10 and from 71.89 mg per g of AC to 46.78 mg per g of AC for pH 4 to 10, respectively.

As illustrated in Fig. 4B, the pH_{pzc} values of AC and KNTs were found to be 5.40 and 7.50, respectively. From these values, the charged surfaces of the adsorbents were positive and negative when $\text{pH} < \text{pH}_{\text{pzc}}$ and $\text{pH} > \text{pH}_{\text{pzc}}$, respectively. Therefore, at pH values below 5.40 and 7.5 (pH_{pzc}), the surface of the activated carbon and kaolin particles are positively charged, respectively. At acidic pH, the functional groups lining the surface of activated carbon and kaolin undergo strong protonation which gives

the material an overall positive charge. Therefore, the PO_4^{3-} ions were surrounded by protonated adsorbents by electrostatic attraction (Zhang et al., 2022). Furthermore, for KNTs, higher PO_4^{3-} removal at pH 2 can be explained by the complexation of the inner sphere of phosphate species on the surface of kaolinite via ligand exchange reaction mechanisms (Ouakouak & Youcef, 2016). When the pH increases, the surface becomes less and less protonated, causing repulsion between the anionic species of PO_4^{3-} and the surface of the activated carbon and kaolin (Das et al., 2021). Moreover, at basic pH, adsorption also decreases through the competition effect of hydroxyl ions (OH^-) (Zhang et al., 2022). A similar trend has been found for the Linthipe kaolinite (Kaminyango

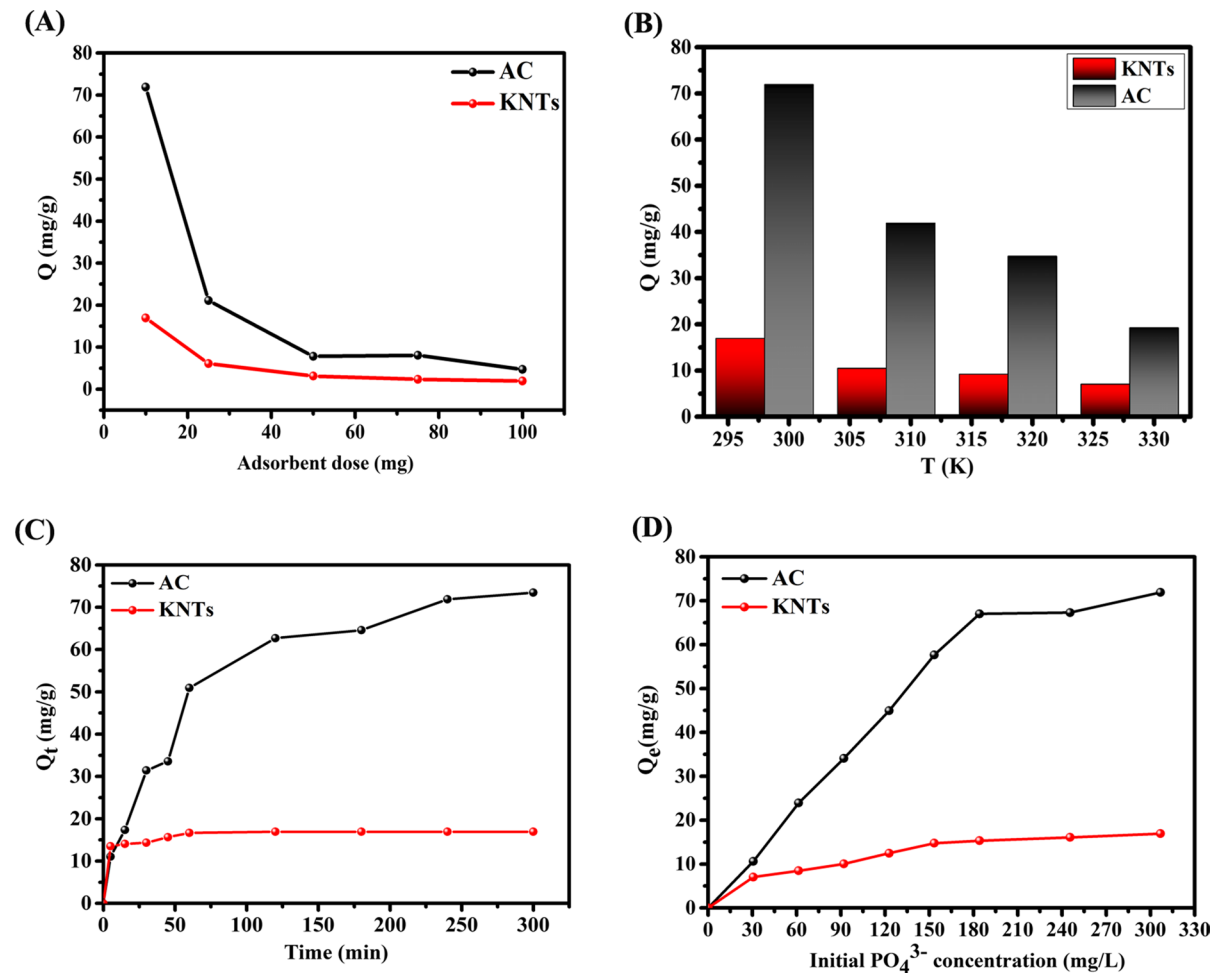


Fig. 5 A Effect of adsorbents dose on phosphate adsorption, (B) Effect of temperature on phosphate adsorption, (C) Adsorption kinetic plots for phosphate on KNTs and AC and

(D) Effect of initial phosphate concentration on the adsorption ability of KNTs and AC

et al., 2009) and for other adsorbents such as lanthanum hydroxide $\text{La}(\text{OH})_3$ (Zhang et al., 2021), lanthanum-zirconium modified iron oxide ($\text{La-Zr@Fe}_3\text{O}_4$) (Lin et al., 2021), Lanthanum modified chitosan-attapulgit (Kong et al., 2023), zirconium/poly(vinyl alcohol)-modified flat-sheet poly-(vinylidene fluoride) membrane (Zhao & Chen, 2016), and bentonite entrapped in Ca-alginate beads (Xu et al., 2020).

3.3 Effect of Adsorbent Dose

The influence of the adsorbent dose was examined within the range of 10 to 100 mg. The results (Fig. 5A) show that, for a fixed concentration of 100 mg/L of phosphate and a contact time of 240 min, increasing the dose of KNTs and AC from 10 to 100 mg leads to a decrease in the amount of phosphate adsorbed, expressed in mg per gram. For instance, the adsorbed amount of phosphate decreases from 71.89 mg/g to 4.69 mg/g for AC, and from 16.93 mg/g to 1.95 mg/g for KNTs, as the dose of the adsorbent increases. This can be attributed to the increase in the number of active binding sites available with higher adsorbent dose, resulting in a higher removal efficiency and a decrease in the remaining phosphate dose in the solution. Nevertheless, the total quantity of PO_4^{3-} in the system remains constant. Therefore, the amount of adsorption per unit mass of the adsorbent is reduced.

Activated carbon showed higher uptake capacity than KNTs, which is due to the high specific surface area of AC. However, at low concentration (10 mg/L), the two adsorbents showed a higher phosphate removal rate of 93.74% for AC and 69% for KNT (Fig. S2).

3.4 Effect of Temperature

Figure 5B showed that the increase in temperature in the interval studied leads to a significance reduction in the adsorption capacity of the adsorbents at equilibrium, which explains that the adsorption process is likely to be exothermic (Fizir et al., 2022b). On the other hand, our study reveals that the adsorption of phosphates is more favorable at ambient temperature (298 K).

3.5 Effect of Adsorption time

Figure 5C showed that the adsorption of phosphate on KNTs and AC increases as the contact time increases. For KNTs, the adsorption is rapid in the first 5 min, with an initial adsorption capacity of 13.48 mg/g. Then, gradually increases up to 60 min, reaching an adsorption capacity of 16.64 mg/g. Finally, it stabilizes in a maximum adsorption capacity of 16.93 mg/g. For AC, the adsorption is fast in the first 60 min, with an adsorption capacity of 50.94 mg/g. It gradually increases up to 240 min, reaching an adsorption capacity of 71.89 mg/g. Finally, it stabilizes in a maximum adsorption capacity of 73.74 mg/g. Therefore, the curve highlight two distinct areas:

- The initial rapid adsorption phase, where the adsorption capacity increases quickly.
- The later phase where the adsorption capacity continues to increase, but at a slower rate until it reaches a maximum and stabilizes after 1 h and 4 h for KNTs and AC, respectively.
- In comparison with AC, the adsorption of PO_4^{3-} ions on KNTs is carried out in a faster way where equilibrium is reached after 60 min and may correspond to a faster ion exchange rate (Hussain & Ali, 2021).

3.6 Effect of Phosphate Concentration

The results revealed that the integration or incorporation of high phosphate concentrations results in an increase in the adsorption capacities of both materials, as shown in Fig. 5D. This suggests that the adsorbing quantities can be controlled to some extent. This trend is noticed until a phosphate concentration of 245 mg/L which was identified as the equilibrium concentration for both adsorbents. The experimental maximum adsorption capacities of KNTs and AC were found to be 16.93 and 71.89 mg/g, respectively. The increase in the adsorption capacities of phosphate by the adsorbents may be due to the induction of higher driving forces when testing high concentrations of phosphate.

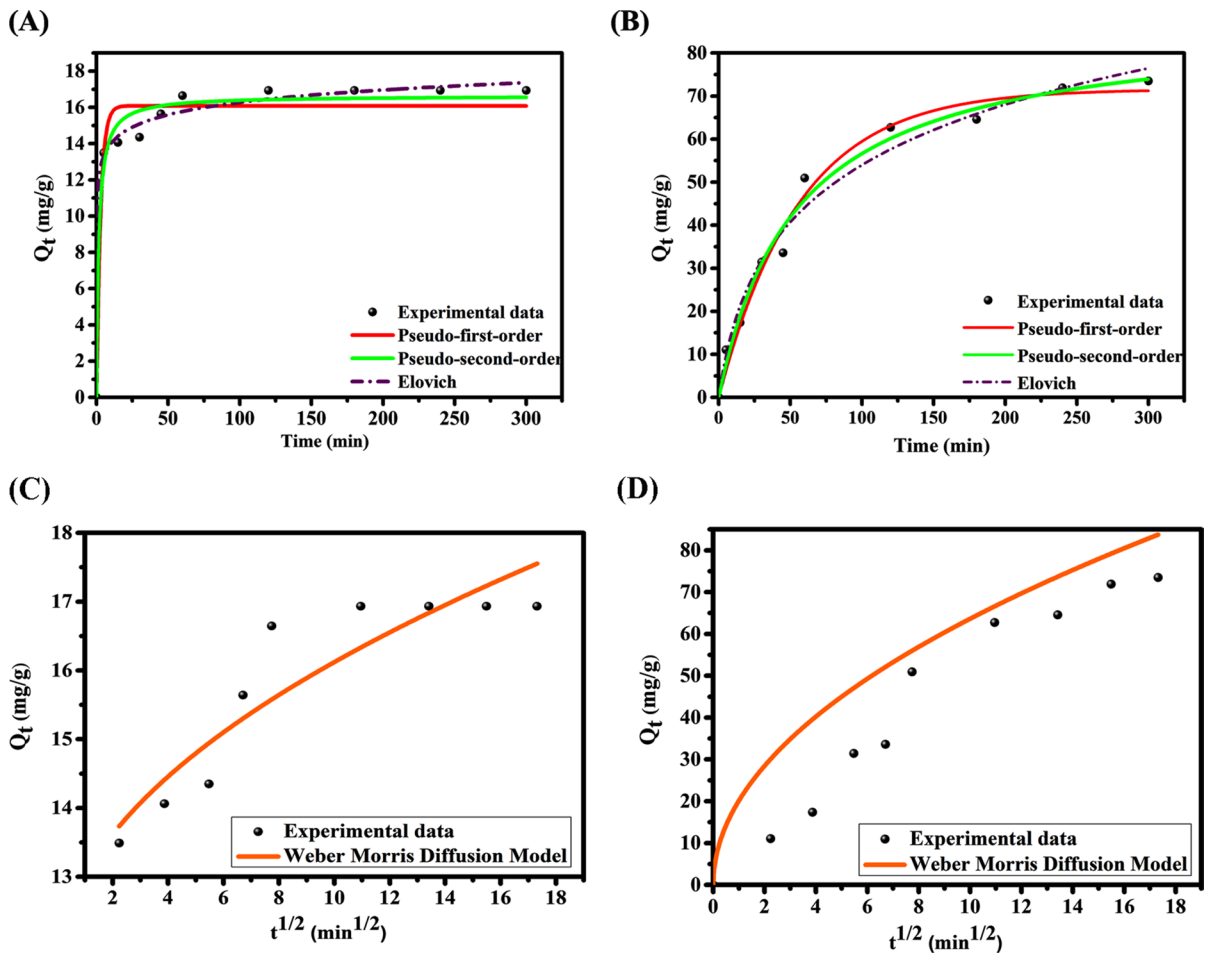


Fig. 6 Nonlinear fitting to kinetic models for the phosphate adsorption by (A) KNTs, and (B) AC; Weber Morris Diffusion model for the phosphate adsorption by (C) KNTs, and (D) AC

3.7 Adsorption Kinetic, Equilibrium, and Thermodynamic Properties

3.7.1 Kinetic Behaviors

The kinetic behaviors of the adsorption processes for the KNTs and AC were illustrated by using the pseudo-first-order model and pseudo-second-order kinetic (Fig. 6). The theoretical parameters of the fitting results are presented in Table 5. The adsorption capacity outcomes of phosphate by KNTs demonstrated significant accord with both pseudo-first-order and pseudo-second-order models ($R^2 > 0.95$, $Q_{ecal} \sim Q_{exp}$), and the kinetic properties of the investigated systems showed a slight preference to be explained

according to the suggestion of the pseudo-second-order model, $R^2 = 0.976$ (Fig. 6 and Table 5) indicating the dominance of the chemisorption mechanisms during the uptake of phosphate, and other support mechanisms that have more physical affinity (physisorption) (Abukhadra et al., 2020). Internal diffusion, surface complexation, electron exchange, and electrostatic interactions may be involved in the both suggested mechanisms. As for AC, the data (R^2 and Q_{ecal}) fitted the best into pseudo-first-order kinetic model which means that physisorption played a significant role in the removal process of PO_4^{3-} onto AC (Hua et al., 2016). As the chemisorption was the dominant mechanism of PO_4^{3-} adsorption by KNTs, and so the Elovich model was applied to explain

Table 5 Kinetic modeling for the phosphate adsorption

Model	Parameters	KNTs	AC
Pseudo-first order	k_1	0.351	0.017
	Q_{eexp}	16.933	71.894
	Q_{ecal}	16.080	71.599
	R^2	0.952	0.982
Pseudo-second order	k_2	0.038	0.018
	Q_{ecal}	16.63	87.278
	R^2	0.976	0.976
Elovich	α	$150.193 \cdot 10^3$	2.420
	β	1.016	0.046
	R^2	0.990	0.977
Weber Morris Intra-Particle Diffusion	k_3	1.432	20.122
	C	11.592	0.000
	R^2	0.815	0.696

Table 6 Equilibrium modeling for adsorption of phosphate onto KNTs and AC

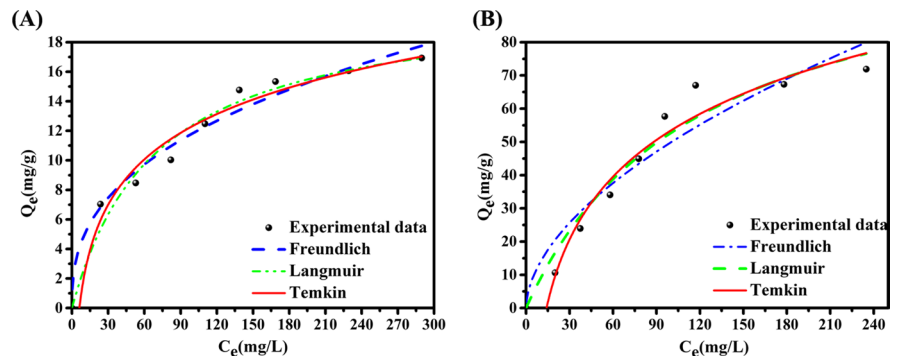
Model	Parameters	KNTs	AC
Langmuir	K_L	0.014	0.008
	Q_{eexp}	16.91	71.894
	Q_m	20.971	115.234
	R^2	0.928	0.926
Freundlich	R_L	0.184–0.693	0.278–0.794
	K_F	2.041	3.918
	$1/n_F$	0.381	0.552
Temkin	R^2	0.940	0.856
	K_T	0.162	0.071
	B	4.421	27.269
	b_T	560.14	90.81
R^2	0.972	0.964	

the chemisorption process in term of variation of chemisorption energetic with the extent of surface coverage (Teng & Hsieh, 1999). The correlation coefficients (R^2) for the Elovich model (Table 5) fitted well with the experimental data for the KNTs (Fig. 6) demonstrating that the adsorption of PO_4^{3-} was controlled by chemisorption onto heterogenous binding sites in the KNTs. Similar findings was observed in previous works (Das et al., 2021).

The Weber Morris Intra-Particle Diffusion Model (Fig. 6) was also examined to gain a better understanding of the adsorption mechanism and the steps that control the rate of the process. In the case of AC (Fig. 6D), the plot of (Q_t) against ($t^{1/2}$) passes through the origin, indicating the adsorption is dominated by the intraparticle

diffusion (Falahian et al., 2018). However, for KNTs (Fig. 6C), the line deviates from the origin, suggesting that intra-particle transport is not the only factor limiting the rate. This indicates that the adsorption of phosphate onto KNTs is a multiple process involving surface adsorption, inter-particle diffusion, and intra-particle diffusion (Wang & Guo, 2022). A similar pattern was observed when examining the adsorption capacity at three different initial concentrations. Initially, there was a gradual increase in adsorption capacity, but it eventually reached a plateau as the process reached equilibrium (Lian et al., 2020). This indicates that there was faster mass transfer through the boundary layer on the surface of KNTs at the beginning of the adsorption process. However, as the process continued, it was controlled by the slower diffusion of the adsorbate inside the KNTs.

Fig. 7 Nonlinear fitting to Langmuir, Freundlich, and Temkin isotherms for phosphate adsorption onto (A) KNTs and (B) AC



3.7.2 Adsorption Isotherm

The non linear fitting results with Langmuir and Freundlich models as well as the Temkin model was depicted in Fig. 7 and the parameters values are presented in Table 6. According to the Langmuir model, adsorption process takes place upon a homogeneous surface where the adsorbate is distributed in monolayers (Wang et al., 2022). Langmuir model showed determination coefficient (R^2) of 0.92 for both adsorbents (Table 6). The dimensionless parameter of the sorption intensity (R_L) in the Langmuir model (Eq. (09)) was determined using the sorption constant K_L and the initial phosphate concentration ($C_0=30\text{--}306 \text{ PO}_4^{3-}\text{-P/L}$) ranged from 0.184 to 0.693 for KNTs and from 0.278–0.794 for AC for different initial phosphate concentrations (Table 6) and that suggests that the phosphate adsorption by KNTs and AC is favorable (Weber & Chakravorti, 1974).

$$R_L = 1/(1 + C_0K_L) \quad (3)$$

Freundlich model is an empirical equation based in the adsorption on a heterogeneous surface with binding sites of different affinities (Fizir et al., 2022b). Freundlich model presented R^2 of 0.94 for KNTs and 0.85 for AC (Table 6). The ratio $1/n_F$ offers the surface heterogeneity information (Das et al., 2021). The $1/n_F$ value was 0.381 for KNTs and 0.552 for

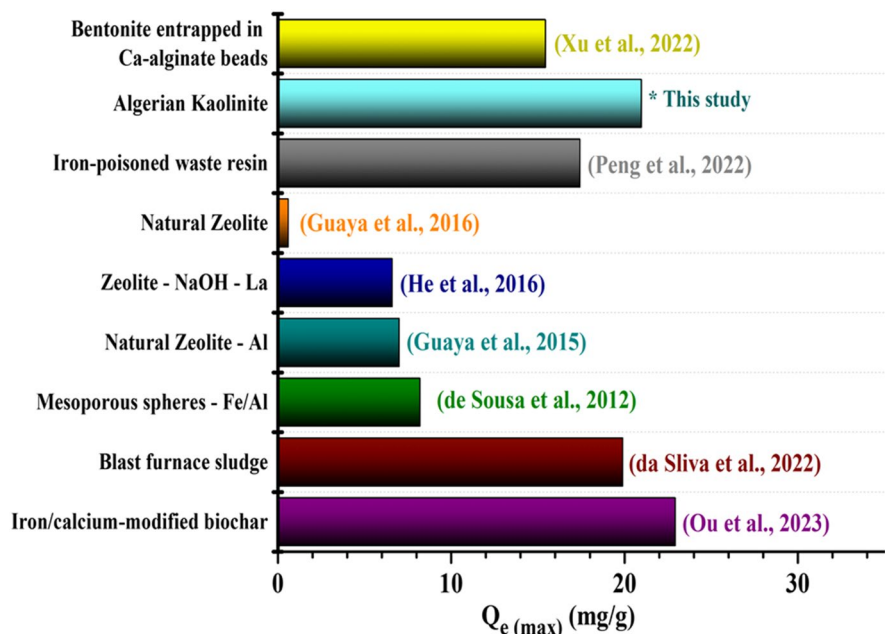
AC signifying that KNTs presents high heterogeneity degree.

Temkin model suggests that the heat of adsorption of all adsorbate molecules diminishes linearly with the coverage of adsorbent due to adsorbent-adsorbate interactions (Hua Huang et al., 2017a, b). Temkin model showed highest R^2 value (>0.95), signifying that this model was best fitted to experimental data (Table 6). The Temkin constant, b_T , is defined as variation of adsorption energy. The b_T values were 560.14 and 90.81 for KNTs and AC, respectively demonstrating that the adsorption reaction of phosphate onto adsorbents may occurs exothermically in the concentration range studied (Hua Huang et al., 2017a, b). The theoretical maximum capacities of KNTs calculated by Langmuir reached 20.97 mg/g (Table 6), which were much competitive among most of the other type of clays-based adsorbents (Fig. 8). such as zeolite (Guaya et al., 2015, 2016; He et al., 2016), and bentonite (Xu et al., 2020), steel industry wastes (da Silva et al., 2022), iron-poisoned waste resin (Peng et al., 2022) and other adsorbents (de Sousa et al., 2012; Ou et al., 2023).

3.8 Thermodynamic Studies

To describe the relationship between surface and temperature, thermodynamic studies was carried out to

Fig. 8 Comparison between the maximum adsorption capacities of KNTs towards phosphate with those recently reported adsorbents



further understand the adsorption process. Standard Gibbs free energy (ΔG°), enthalpy (ΔH°) and entropy (ΔS°) were using the following equations (Van't Hoff equation) (Sereshti et al., 2020; Sevim et al., 2021; Yadav et al., 2022):

$$K = \frac{Q_e}{C_e} \tag{4}$$

$$\Delta G^\circ = -RT \cdot \ln K \tag{5}$$

$$\ln K = \left(\frac{\Delta S^\circ}{R} \right) - \left(\frac{\Delta H^\circ}{R} \right) \frac{1}{T} \tag{6}$$

$$\Delta G^\circ = \Delta H^\circ - T \Delta S^\circ \tag{7}$$

where:

K is the equilibrium constant (the calculation process of this parameter is presented in SI).

R is an ideal gas constant (8.314 J/mol K).

According to Fig. 9, it is observed that the natural logarithm of the equilibrium constant ($\ln K$) decreases as the temperature increases. This implies that the adsorption efficiency is preferable at ambient temperature, as indicated by the findings of (Sereshti et al., 2020). According to Table 7, the positive values of ΔG° indicate that the adsorption of phosphate by the studied adsorbents is not spontaneous. The determined standard Gibbs free energy values for phosphate adsorption fall between 0 and -20 kJ/mol which suggests that the adsorption of phosphate onto both adsorbents is a physical adsorption process (Kiomarsipour et al., 2021). In another hand, the values of

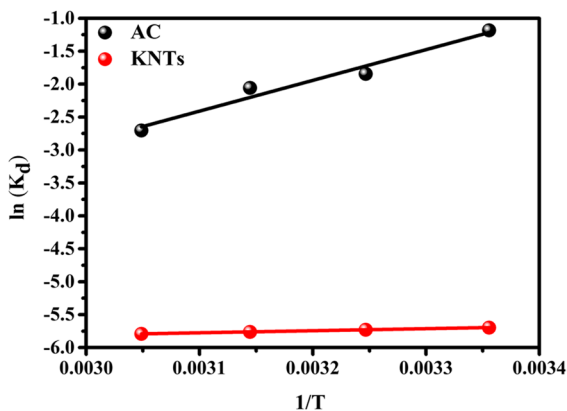


Fig. 9 Plot of $\ln K$ vs $1/T$

Table 7 Thermodynamic parameters

	T (K)	ΔG° (KJ/mol)	ΔH° (KJ/mol)	ΔS° (J/(K.mol))
KNTs	298	14.106	-2.596	-56.0512
	308	14.667		
	318	15.227		
	328	15.788		
AC	298	3.011	-38.795	-140.2915
	308	4.414		
	318	5.816		
	328	7.219		

ΔG° found to be decrease at low temperatures, which means that the adsorption becomes more favorable at lower temperatures. The negative value of ΔH° indicates that the adsorption is exothermic. The negative values of entropy proved that the adsorption is also exothermic and that there is a decrease in the degree of randomness at the solid–liquid interface during the adsorption process.

3.9 Regeneration Studies

Figure 10 shows the regeneration capacities of KNTs and AC over 4 permanent adsorption–desorption process. After 3 cycles, the phosphate adsorption capacity reduced by 12.69% (14.78 mg/g compared to the original, 16.93 mg/g) which proved the adsorption capability did not reduced noticeably, and the KNTs can keep stable in the water samples

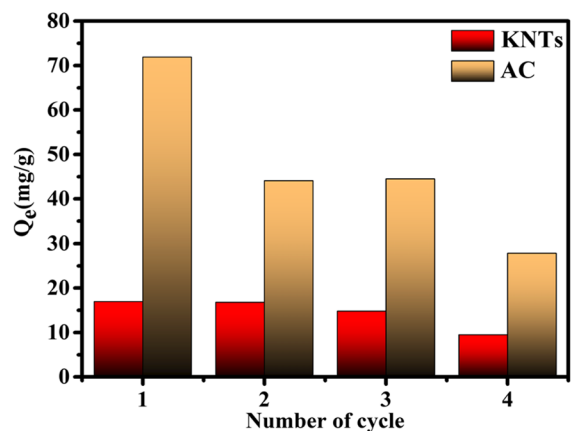


Fig. 10 Reusability of the sorbents

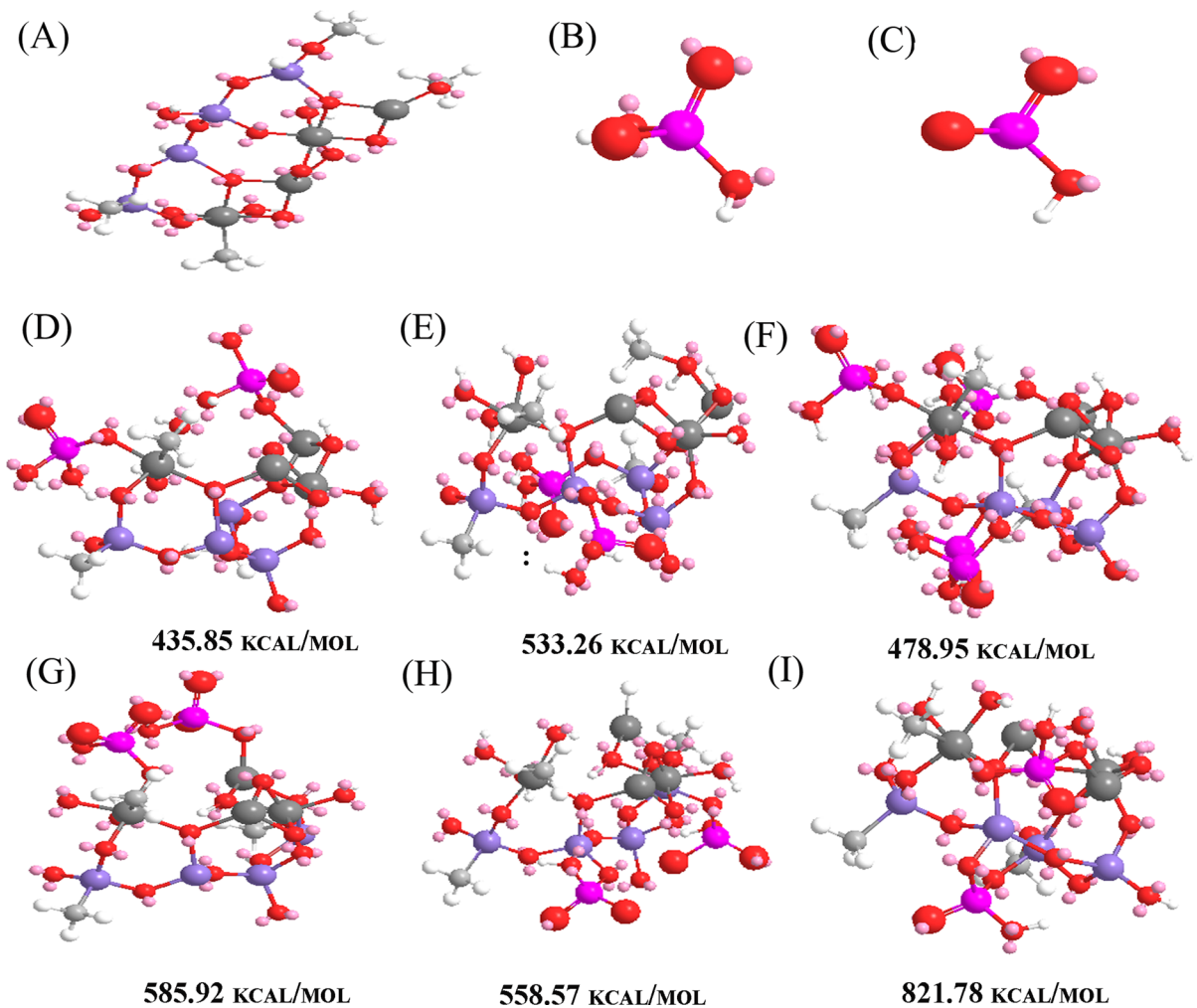


Fig. 11 Proposed surface complexation interactions configurations and interaction energy for H_2PO_4^- (B, D–F) and HPO_4^{2-} (C, G–I) on the surface of kaolinite (A)

with a good ability of recycling. In contrast, the loading capacity of AC significantly reduced by 61.87% (44.48 mg/g compared to the original, 71.89 mg/g, demonstrating that KNTs is efficiently practical on a large scale.

3.10 Phosphate Adsorption Mechanism and CHEM3D Analysis

To elucidate the interaction mode between the KNTs with phosphate, the binding energies of phosphate molecules with the KNTs interface was computed by using CHEM3D. Generally, the H_2PO_4^- or HPO_4^{2-} were the dominant structure of phosphate in wastewater at pH

2–12 which are used to calculate their binding interactions with KNTs. The 3D molecule structures were studied after MM2 optimizations (Jawla & Kumar, 2013) (Fig. 11). The interaction energies (E_{int} , kcal/mol) of H_2PO_4^- or HPO_4^{2-} on the surface of KNTs were calculated with Eq. (08) (Kumar & Viswanathan, 2017):

$$E_{\text{int}} = E(\text{AB}) - (E(\text{A}) + E(\text{B})) \quad (8)$$

where $E(\text{AB})$ is the total energies of KNTs adsorbed to H_2PO_4^- or HPO_4^{2-} , and $E(\text{A})$ and $E(\text{B})$ is the energies of the adsorbate H_2PO_4^- or HPO_4^{2-} and the adsorbent of KNTs, respectively.

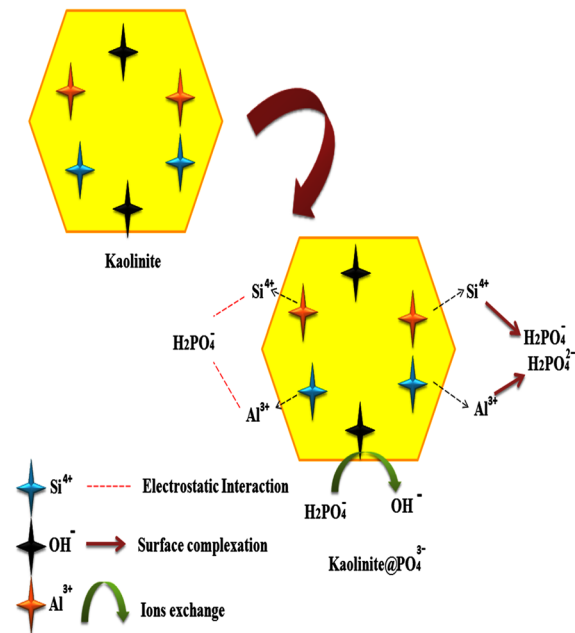


Fig. 12 Global adsorption mechanism of phosphate

Dihydrogen phosphate (H₂PO₄⁻) or HPO₄²⁻ may form complexation with the KNTs surface via ligand exchange reaction mechanisms represented by the Eqs. 09, 10, 11, 12 or 13 (Xu et al., 2020; Zhang et al., 2022) and potential binding structures of phosphate with KNTs is displayed in Fig. 11. Distinctly, there are three configurations for phosphate binding with KNTs. First configuration is represented by the interaction of H₂PO₄⁻ (Fig. 11D) or HPO₄²⁻ (Fig. 11G) with Si (Si-P), the second configuration is represented by the interaction of H₂PO₄⁻ (Fig. 11E) or HPO₄²⁻ (Fig. 11H) with Al (Al-P) and the third configuration is represented by the interaction of H₂PO₄⁻ (Fig. 11F) or HPO₄²⁻ (Fig. 11I) with both Si and Al groups. Generally, the higher absolute value of E_{int} represents the strong affinity of the adsorbent surface to the target contaminant, which is more beneficial to the adsorption of phosphate (Wang et al., 2022). As illustrated in Fig. 11, positive E_{int} was the most preferential characteristic of the configurations, which correspond to the interaction and attraction orientation of H₂PO₄⁻ and HPO₄²⁻ with KNTs. It can be seen that phosphate

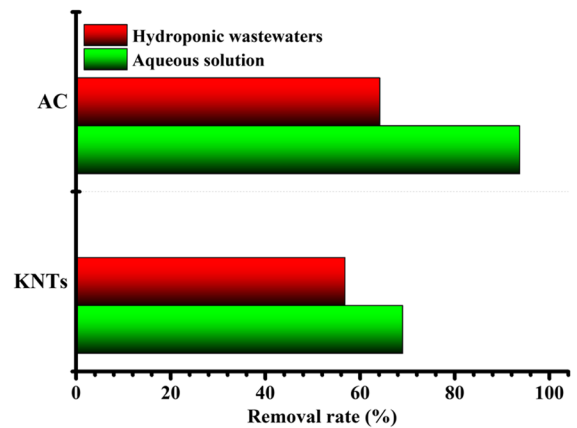
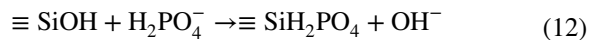
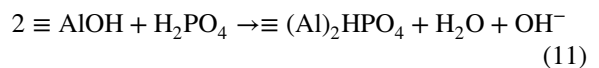


Fig. 13 Removal capacity of KNTs and AC toward phosphate in hydroponic wastewaters

with more charged (HPO₄²⁻), showed greater E_{int} than H₂PO₄⁻, which indicated that HPO₄²⁻ interaction with KNTs are more stable.



Combined with the batch adsorption experiments, and CHEM3D analysis (theoretical calculations), the dominant interaction mechanism for adsorption of phosphate by KNTs may be hypothesized as Fig. 12 where the electrostatic interaction, ion exchange and surface complexation may be formed during the adsorption of phosphates by the KNTs. The mobility of HPO₄²⁻ /H₂PO₄⁻/PO₄³⁻ in solution would be the fastest towards protonated Al-OH⁴⁺ and Si-OH⁵⁺ in order to form the electrostatic bond (Kumar & Viswanathan, 2020). This electrostatic adsorption was further elucidated by the pH study discussed earlier. The interstitial OH⁻ ions of kaolin clay can be exchanged for phosphate ions by an ion exchange mechanism (Li et al., 2016).

3.11 Feasibility of Phosphate Removal From Hydroponic Wastewater

As shown in Fig. 13, utilization of KNTs and AC to remove phosphate at low concentration from the real hydroponic wastewaters polluted by phosphate and other elements (Table S1) resulted in 56.81% and 64.19% removal, respectively, after 60 min. These values were lower than those obtained using aqueous solution; this dissimilarity might be attributed to the coexisting-ions effects such as nitrates, and ammonium among others, in real water samples (Eltaweil et al., 2023). The generally good removal efficiency of phosphate described above suggests that KNTs is a good substitute to AC in term of removal efficiency and might have an application potential in remediating the phosphate contaminated wastewater.

4 Conclusion

In this research, adsorption capacity of Algerian KNTs toward phosphate ions was studied and compared to those of commercial AC. The FTIR analyses revealed the successful adsorption of phosphate on both adsorbents. Batch experiment studies showed that KNTs was efficient in phosphate removal and had an acceptable phosphate uptake capacity (16.93 mg/g). However, the two adsorbents showed a higher phosphate removal rate of 93.74% for AC and 69% for KNTs. The adsorption of phosphate by KNTs and AC showed a high pH dependency where the adsorbents could efficiently eliminate phosphate in the pH range from 2 to 4, indicating that the electrostatic attraction is among the dominant adsorption mechanism. The phosphate adsorption process on KNTs followed both the pseudo-first-order and pseudo-second-order kinetic model and Temkin isotherm model fitted well with the experimental data. The thermodynamic parameters demonstrated that the adsorption of phosphate was probably exothermic in nature. Adsorption/desorption experiments confirmed that KNTs has a higher reproducibility than AC. Molecular modeling study confirmed that phosphate with more charged (HPO_4^{2-}), showed greater E_{int} than H_2PO_4^- , which indicated that HPO_4^{2-} interaction with KNTs are more stable and suggested that electrostatic interaction, and inner-sphere complexation processes were the dominant adsorption mechanism.

The field applicability study in real hydroponic wastewaters further indicated the application potential of KNTs. This research offered promising candidates for real water purification against phosphate contamination. Furthermore, the possible valorization of Algerian KNTs@ PO_4^{3-} as economic slow release fertilizers to soil should be investigated in the future as it may use less amounts of fertilizers based NPK. Overall, the results indicated that, KNTs is a good adsorbent of phosphate. However, it is not superior to AC in terms of adsorption capacity.

Acknowledgements This paper is funded by the PRIMA programme that is supported by the European Union under Grant Agreement No. 1821, WATERMED 4.0, Call 2018 Sect. 1 Water. We appreciate the support provided by Ministry of Higher Education and Scientific Research (Algeria) and General Directorate for Scientific Research and Technological Development (DGRSDT).

Data Availability The data that support the findings of this study are available from the corresponding author upon reasonable request.

Declaration

Competing Interest The authors declare that they have no known competing interests.

References

- Abukhadra, M. R., Refay, N. M., El-Sherbeeney, A. M., & El-Meligy, M. A. (2020). Insight into the loading and release properties of MCM-48/biopolymer composites as carriers for 5-fluorouracil: Equilibrium modeling and pharmacokinetic studies. *ACS Omega*, 5(20), 11745–11755.
- Alahabadi, A., Hosseini-Bandegharai, A., Moussavi, G., Amin, B., Rastegar, A., Karimi-Sani, H., & Miri, M. (2017). Comparing adsorption properties of NH_4Cl -modified activated carbon towards chlortetracycline antibiotic with those of commercial activated carbon. *Journal of Molecular Liquids*, 232, 367–381.
- Ali, M. E., Zaghlool, E., Khalil, M., & Kotp, Y. (2022). Surface and internal modification of composite ion exchange membranes for removal of molybdate, phosphate, and nitrate from polluted groundwater. *Arabian Journal of Chemistry*, 15(4), 103747.
- Almasri, D. A., Saleh, N. B., Atieh, M. A., McKay, G., & Ahzi, S. (2019). Adsorption of phosphate on iron oxide doped halloysite nanotubes. *Scientific Reports*, 9(1), 3232.
- Al-Zboon, K. K. (2018). Phosphate removal by activated carbon-silica nanoparticles composite, kaolin, and olive cake. *Environment, Development and Sustainability*, 20(6), 2707–2724.

- Awad, M. E., López-Galindo, A., Setti, M., El-Rahmany, M. M., & Iborra, C. V. (2017). Kaolinite in pharmaceuticals and biomedicine. *International Journal of Pharmaceutics*, 533(1), 34–48.
- Biniak, S., Szymański, G., Siedlewski, J., & Świątkowski, A. (1997). The characterization of activated carbons with oxygen and nitrogen surface groups. *Carbon*, 35(12), 1799–1810.
- da Silva, J. M., da Silva, C. E., Freire, J. M., Becker, H., Diógenes, I. C., & Longhinotti, E. (2022). Industrial steel waste-based adsorbent: An effective phosphate removal from aqueous media. *Materials Chemistry and Physics*, 292, 126828.
- Das, T. K., Scott, Q., & Bezbaruah, A. N. (2021). Montmorillonite-iron crosslinked alginate beads for aqueous phosphate removal. *Chemosphere*, 281, 130837.
- de Sousa, A. F., Braga, T. P., Gomes, E. C. C., Valentini, A., & Longhinotti, E. (2012). Adsorption of phosphate using mesoporous spheres containing iron and aluminum oxide. *Chemical Engineering Journal*, 210, 143–149.
- Debbaudt, A. L., Ferreira, M. L., & Gschaidner, M. E. (2004). Theoretical and experimental study of M2+ adsorption on biopolymers. III. Comparative kinetic pattern of Pb, Hg and Cd. *Carbohydrate Polymers*, 56(3), 321–332.
- Dewi, R., Agusnar, H., & Alfian, Z. (2018). Characterization of technical kaolin using XRF, SEM, XRD, FTIR and its potentials as industrial raw materials. *Journal of Physics: Conference Series*, 1116(4), 042010.
- Elmsellem, H., Elgadi, M., & Kolli, M. (2013). Synthèse du phosphate tricalcique apatitique et sa céramisation en [Beta]-TCP. *Nature & Technology*, 8, 2.
- Eltaweil, A. S., Ibrahim, K., Abd El-Monaem, E. M., El-Subruiti, G. M., & Omer, A. M. (2023). Phosphate removal by Lanthanum-doped aminated graphene oxide@ aminated chitosan microspheres: Insights into the adsorption mechanism. *Journal of Cleaner Production*, 385, 135640.
- Falahian, Z., Toriki, F., & Faghian, H. (2018). Synthesis and application of polypyrrole/Fe3O4 nanosize magnetic adsorbent for efficient separation of Hg2+ from aqueous solution. *Global Challenges*, 2(1), 1700078.
- Fan, H.-T., Shi, L.-Q., Shen, H., Chen, X., & Xie, K.-P. (2016). Equilibrium, isotherm, kinetic and thermodynamic studies for removal of tetracycline antibiotics by adsorption onto hazelnut shell derived activated carbons from aqueous media. *RSC Advances*, 6(111), 109983–109991.
- Fizir, M., Wei, L., Muchuan, N., Itatahine, A., Mehdi, Y. A., He, H., & Dramou, P. (2018). QbD approach by computer aided design and response surface methodology for molecularly imprinted polymer based on magnetic halloysite nanotubes for extraction of norfloxacin from real samples. *Talanta*, 184, 266–276. <https://doi.org/10.1016/j.talanta.2018.02.056>
- Fizir, M., Liu, W., Tang, X., Wang, F., & Benmokadem, Y. (2022a). Design approaches, functionalization, and environmental and analytical applications of magnetic halloysite nanotubes: A review. *Clays and Clay Minerals*, 70, 660–694.
- Fizir, M., Richa, A., Touil, S., Benmokadem, Y., Boubekeur, K., Hallal, B., & Wei, L. (2022b). Preparation and application of a surfactant-modified Halloysite nanotubes for the adsorption of nitrates from aqueous solutions: Kinetic and equilibrium studies. *Environmental Progress & Sustainable Energy*, 42, e13995.
- Gagnon, V., Maltais-Landry, G., Puigagut, J., Chazarenc, F., & Brisson, J. (2010). Treatment of hydroponics wastewater using constructed wetlands in winter conditions. *Water, Air, & Soil Pollution*, 212, 483–490.
- Ge, I. T. K., Nugraha, M. W., Kamal, N. A., & Sambudi, N. S. (2019). Composite of kaolin/sodium alginate (SA) beads for methylene blue adsorption. *ASEAN Journal of Chemical Engineering*, 19(2), 100–109.
- Guaya, D., Valderrama, C., Farran, A., Armijos, C., & Cortina, J. L. (2015). Simultaneous phosphate and ammonium removal from aqueous solution by a hydrated aluminum oxide modified natural zeolite. *Chemical Engineering Journal*, 271, 204–213.
- Guaya, D., Valderrama, C., Farran, A., & Cortina, J. L. (2016). Modification of a natural zeolite with Fe (III) for simultaneous phosphate and ammonium removal from aqueous solutions. *Journal of Chemical Technology & Biotechnology*, 91(6), 1737–1746.
- He, Y., Lin, H., Dong, Y., Liu, Q., & Wang, L. (2016). Simultaneous removal of ammonium and phosphate by alkaline-activated and lanthanum-impregnated zeolite. *Chemosphere*, 164, 387–395.
- Hosseinzadeh, S., Bonarrigo, G., Verheust, Y., Roccaro, P., & Van Hulle, S. (2017). Water reuse in closed hydroponic systems: Comparison of GAC adsorption, ion exchange and ozonation processes to treat recycled nutrient solution. *Aquacultural Engineering*, 78, 190–195.
- Hosseinzadeh, S., Liu, Z., De Graeve, J., BKheet, M., Libbrecht, W., De Clercq, J., & Van Hulle, S. (2019). Recirculating water treatment in closed hydroponic systems: assessment of granular activated carbon and soft templated mesoporous carbon for adsorptive removal of root exudates. *Environmental Processes*, 6, 1–23.
- Hu, Q., He, L., Lan, R., Feng, C., & Pei, X. (2022). Recent advances in phosphate removal from municipal wastewater by electrocoagulation process: A review. *Separation and Purification Technology*, 308(17), 122944.
- Hua, G., Salo, M. W., Schmit, C. G., & Hay, C. H. (2016). Nitrate and phosphate removal from agricultural subsurface drainage using laboratory woodchip bioreactors and recycled steel byproduct filters. *Water Research*, 102, 180–189.
- Huang, H., Liu, J., Zhang, P., Zhang, D., & Gao, F. (2017a). Investigation on the simultaneous removal of fluoride, ammonia nitrogen and phosphate from semiconductor wastewater using chemical precipitation. *Chemical Engineering Journal*, 307, 696–706.
- Huang, H., Tang, J., Gao, K., He, R., Zhao, H., & Werner, D. (2017b). Characterization of KOH modified biochars from different pyrolysis temperatures and enhanced adsorption of antibiotics. *RSC Advances*, 7(24), 14640–14648.
- Huang, X., Huang, K., Wang, S., Cao, Z., & Zhong, H. (2019). Synthesis of 2-hydroxyethyl dibutylidithiocarbamate and its adsorption mechanism on chalcocopyrite. *Applied Surface Science*, 476, 460–467.
- Hussain, S. T., & Ali, S. A. K. (2021). Removal of heavy metal by ion exchange using bentonite clay. *Journal of Ecological Engineering*, 22(1), 104–111.
- Isiuku, B. O., & Enyoh, C. E. (2020). Pollution and health risks assessment of nitrate and phosphate concentrations in water bodies in South Eastern. *Nigeria. Environmental Advances*, 2, 100018.

- Jawla, S., & Kumar, Y. (2013). Study of QSAR descriptors of antihyperglycemic principle pinitol using computation servers. *Middle-East Journal of Scientific Research*, 16(5), 587–594.
- Kamiyango, M., Masamba, W., Sajidu, S., & Fabiano, E. (2009). Phosphate removal from aqueous solutions using kaolinite obtained from Linthipe, Malawi. *Physics and Chemistry of the Earth, Parts a/b/c*, 34(13–16), 850–856.
- Khan, A. M., Shafiq, F., Khan, S. A., Ali, S., Ismail, B., Hakeem, A. S., & Khan, A. R. (2019). Surface modification of colloidal silica particles using cationic surfactant and the resulting adsorption of dyes. *Journal of Molecular Liquids*, 274, 673–680.
- Kiomarsipour, N., Alizadeh, M., & Ghani, K. (2021). Synthesis and surface-functionalizing of ordered mesoporous carbon CMK-3 for removal of nitrate from aqueous solution as an effective adsorbent. *Diamond and Related Materials*, 116, 108419.
- Konadu-Amoah, B., Hu, R., Ndé-Tchoupé, A. I., Gwenzi, W., & Noubactep, C. (2022). Metallic iron (Fe⁰)-based materials for aqueous phosphate removal: A critical review. *Journal of Environmental Management*, 315, 115157.
- Kong, L., Tian, Y., Pang, Z., Huang, X., Li, M., Yang, R., & Zuo, W. (2019). Synchronous phosphate and fluoride removal from water by 3D rice-like lanthanum-doped La@MgAl nanocomposites. *Chemical Engineering Journal*, 371, 893–902.
- Kong, H., Li, Q., Zheng, X., Chen, P., Zhang, G., & Huang, Z. (2023). Lanthanum modified chitosan-attapulgitite composite for phosphate removal from water: Performance, mechanisms and applicability. *International Journal of Biological Macromolecules*, 224, 984–997.
- Kumar, I. A., & Viswanathan, N. (2017). Development of multivalent metal ions imprinted chitosan biocomposites for phosphate sorption. *International Journal of Biological Macromolecules*, 104, 1539–1547.
- Kumar, I. A., & Viswanathan, N. (2020). Fabrication of zirconium (IV) cross-linked alginate/kaolin hybrid beads for nitrate and phosphate retention. *Arabian Journal of Chemistry*, 13(2), 4111–4125.
- Lee, J.-H., Velmurugan, P., Ravi, A. V., & Oh, B.-T. (2020). Green and hydrothermal assembly of reduced graphene oxide (rGO)-coated ZnO and Fe hybrid nanocomposite for the removal of nitrate and phosphate. *Environmental Chemistry and Ecotoxicology*, 2, 141–149.
- Li, R., Wang, J. J., Zhou, B., Awasthi, M. K., Ali, A., Zhang, Z., & Mahar, A. (2016). Enhancing phosphate adsorption by Mg/Al layered double hydroxide functionalized biochar with different Mg/Al ratios. *Science of The Total Environment*, 559, 121–129.
- Li, J., Cao, L., Li, B., Huang, H., Yu, W., Sun, C., & Young, B. (2023). Utilization of activated sludge and shell wastes for the preparation of Ca-loaded biochar for phosphate removal and recovery. *Journal of Cleaner Production*, 382, 135395.
- Lian, Q., Yao, L., Uddin Ahmad, Z., Gang, D. D., Kong-gidinata, M. I., Gallo, A. A., & Zappi, M. E. (2020). Enhanced Pb (II) adsorption onto functionalized ordered mesoporous carbon (OMC) from aqueous solutions: The important role of surface property and adsorption mechanism. *Environmental Science and Pollution Research*, 27, 23616–23630.
- Lin, X., Xie, Y., Lu, H., Xin, Y., Altaf, R., Zhu, S., & Liu, D. (2021). Facile preparation of dual La-Zr modified magnetite adsorbents for efficient and selective phosphorus recovery. *Chemical Engineering Journal*, 413, 127530.
- Liu, B., Dai, S., Zhang, X., Cui, F., Nan, J., & Wang, W. (2022). Highly efficient and reusable lanthanum-carbon nanotube films for enhanced phosphate removal. *Separation and Purification Technology*, 299, 121710.
- Loh, C. Y., Lau, W. J., Koe, A. Z. Y., Lim, W. J., & Ooi, B. S. (2022). Simultaneous phosphate recovery and sodium removal from brackish aquaculture effluent via diafiltration-nanofiltration process. *Chemosphere*, 307, 136104.
- Manna, A., Naskar, N., Sen, K., & Banerjee, K. (2022). A review on adsorption mediated phosphate removal and recovery by biomatrices. *Journal of the Indian Chemical Society*, 99(10), 100682.
- Murray, H. H. (2006). Kaolin applications. *Developments in Clay Science*, 2, 85–109.
- Mustapha, S., Ndamitso, M., Abdulkareem, A., Tijani, J., Mohammed, A., & Shuaib, D. (2019). Potential of using kaolin as a natural adsorbent for the removal of pollutants from tannery wastewater. *Heliyon*, 5(11), e02923.
- Mustapha, S., Tijani, J., Ndamitso, M., Abdulkareem, A., Shuaib, D., & Mohammed, A. (2021). Adsorptive removal of pollutants from industrial wastewater using mesoporous kaolin and kaolin/TiO₂ nanoadsorbents. *Environmental Nanotechnology, Monitoring & Management*, 15, 100414.
- Nagul, E. A., McKelvie, I. D., Worsfold, P., & Kolev, S. D. (2015). The molybdenum blue reaction for the determination of orthophosphate revisited: Opening the black box. *Analytica Chimica Acta*, 890, 60–82.
- Nie, G., Liu, X., Li, X., Meng, C., Wang, W., & Zou, D. (2023). Efficient phosphate removal and recovery by using nanosized La (III) oxides anchored on aminated biomass waste. *Separation and Purification Technology*, 305, 122513.
- Ou, W., Lan, X., Guo, J., Cai, A., Liu, P., Liu, N., & Lei, Y. (2023). Preparation of iron/calcium-modified biochar for phosphate removal from industrial wastewater. *Journal of Cleaner Production*, 383, 135468.
- Ouakouak, A., & Youcef, L. (2016). Phosphates removal by activated carbon. *Sensor Letters*, 14(6), 600–605.
- Owodunni, A. A., Ismail, S., Kurniawan, S. B., Ahmad, A., Imron, M. F., & Abdullah, S. R. S. (2023). A review on revolutionary technique for phosphate removal in wastewater using green coagulant. *Journal of Water Process Engineering*, 52, 103573.
- Park, J.-H., Kim, S.-H., Delaune, R. D., Cho, J.-S., Heo, J.-S., Ok, Y. S., & Seo, D.-C. (2015). Enhancement of nitrate removal in constructed wetlands utilizing a combined autotrophic and heterotrophic denitrification technology for treating hydroponic wastewater containing high nitrate and low organic carbon concentrations. *Agricultural Water Management*, 162, 1–14.
- Park, J.-H., Wang, J. J., Kim, S.-H., Cho, J.-S., Kang, S.-W., Delaune, R. D., & Seo, D.-C. (2017). Phosphate removal in constructed wetland with rapid cooled basic oxygen furnace slag. *Chemical Engineering Journal*, 327, 713–724.

- Patel, H. (2021). Review on solvent desorption study from exhausted adsorbent. *Journal of Saudi Chemical Society*, 25(8), 101302.
- Peng, X., Zeng, W., Miao, H., Lu, S., & Li, S. (2022). A novel carbon adsorbent derived from iron-poisoned waste resin for phosphate removal from wastewater: Performance and mechanism. *Process Safety and Environmental Protection*, 168, 324–335.
- Ren, L., Xu, J., Dai, R., & Wang, Z. (2022). Electrochemical removal and recovery of phosphorus from wastewater using cathodic membrane filtration reactor. *Chinese Chemical Letters*, 34(4), 107707.
- Richa, A., Touil, S., Fizir, M., & Martinez, V. (2020). Recent advances and perspectives in the treatment of hydroponic wastewater: A review. *Reviews in Environmental Science and Bio/Technology*, 19, 945–966.
- Seminskaya, O., Balakina, M., & Kucheruk, D. (2017). Processing of retentates of reverse osmosis treatment of phosphate-containing wastewater. *Journal of Water Chemistry and Technology*, 39, 171–176.
- Sereshti, H., Zamiri Afsharian, E., Esmaeili Bidhendi, M., Rashidi Nodeh, H., Afzal Kamboh, M., & Yilmaz, M. (2020). Removal of phosphate and nitrate ions aqueous using strontium magnetic graphene oxide nanocomposite: Isotherms, kinetics, and thermodynamics studies. *Environmental Progress & Sustainable Energy*, 39(2), e13332.
- Sevim, F., Lacin, O., Ediz, E. F., & Demir, F. (2021). Adsorption capacity, isotherm, kinetic, and thermodynamic studies on adsorption behavior of malachite green onto natural red clay. *Environmental Progress & Sustainable Energy*, 40(1), e13471.
- Shao, Y., Li, J., Fang, X., Yang, Z., Qu, Y., Yang, M., & Wang, H. (2022). Chemical modification of bamboo activated carbon surface and its adsorption property of simultaneous removal of phosphate and nitrate. *Chemosphere*, 287, 132118.
- Shu, J., Cheng, S., Xia, H., Zhang, L., Peng, J., Li, C., & Zhang, S. (2017). Copper loaded on activated carbon as an efficient adsorbent for removal of methylene blue. *RSC Advances*, 7(24), 14395–14405.
- Tao, R., Qu, M., Zhang, S., Quan, F., Zhang, M., Shen, W., & Mei, Y. (2022). Preparation of FeOOH supported by melamine sponge and its application for efficient phosphate removal. *Journal of Environmental Chemical Engineering*, 10(4), 108064.
- Teng, H., & Hsieh, C.-T. (1999). Activation energy for oxygen chemisorption on carbon at low temperatures. *Industrial & Engineering Chemistry Research*, 38(1), 292–297.
- Wang, J., & Guo, X. (2022). Rethinking of the intraparticle diffusion adsorption kinetics model: Interpretation, solving methods and applications. *Chemosphere*, 309, 136732.
- Wang, G., Yue, X., Zhang, S., Geng, Q., Zheng, J., Xu, X., & Jia, Y. (2022). La (III) loaded Fe (III) cross-linked chitosan composites for efficient removal of phosphate from wastewater: Performance and mechanisms. *Journal of cleaner production*, 379, 134833.
- Weber, T. W., & Chakravorty, R. K. (1974). Pore and solid diffusion models for fixed-bed adsorbers. *AIChE Journal*, 20(2), 228–238.
- Xu, X., Wang, B., Tang, H., Jin, Z., Mao, Y., & Huang, T. (2020). Removal of phosphate from wastewater by modified bentonite entrapped in Ca-alginate beads. *Journal of Environmental Management*, 260, 110130.
- Xuechu, C., Hainan, K., Deyi, W., Xinze, W., & Yongyong, L. (2009). Phosphate removal and recovery through crystallization of hydroxyapatite using xonotlite as seed crystal. *Journal of Environmental Sciences*, 21(5), 575–580.
- Yadav, S., Yadav, A., Bagotia, N., Sharma, N., Sharma, A. K., & Kumar, S. (2022). Simultaneous adsorption of three anionic dyes at neutral pH from their individual and multi-component systems on a CTAB modified Pennisetum glaucum based carbon nanotube green composite: Adsorption mechanism and process optimization by Box-Behnken design model. *Journal of Molecular Liquids*, 358, 119223.
- Yang, B., Han, F., Bai, Y., Xie, Z., Shi, T., Wang, J., & Li, Y. (2023). Phosphate removal performance and mechanism of magnesium–lanthanum-modified coal gasification coarse slag. *Materials Today Sustainability*, 22, 100357.
- Yoo, S.-H., Lee, S.-C., Jang, H.-Y., & Kim, S.-B. (2023). Characterization of ibuprofen removal by calcined spherical hydrochar through adsorption experiments, molecular modeling, and artificial neural network predictions. *Chemosphere*, 311, 137074.
- Zhang, L., Liu, Y., Wang, Y., Li, X., & Wang, Y. (2021). Investigation of phosphate removal mechanisms by a lanthanum hydroxide adsorbent using p-XRD. *FTIR and XPS. Applied Surface Science*, 557, 149838.
- Zhang, P., He, M., Huo, S., Li, F., & Li, K. (2022). Recent progress in metal-based composites toward adsorptive removal of phosphate: Mechanisms, behaviors, and prospects. *Chemical Engineering Journal*, 446, 137081.
- Zhang, L., Huang, X., Fu, G., & Zhang, Z. (2023). Aerobic electrotrophic denitrification coupled with biologically induced phosphate precipitation for nitrogen and phosphorus removal from high-salinity wastewater: Performance, mechanism, and microbial community. *Bioresource Technology*, 390, 128696.
- Zhao, D., & Chen, J. P. (2016). Application of zirconium/PVA modified flat-sheet PVDF membrane for the removal of phosphate from aqueous solution. *Industrial & Engineering Chemistry Research*, 55(24), 6835–6844.
- Zhao, Y., Geng, J., Wang, X., Gu, X., & Gao, S. (2011). Tetracycline adsorption on kaolinite: PH, metal cations and humic acid effects. *Ecotoxicology*, 20(5), 1141–1147.
- Zheng, S., Fan, J., & Lu, X. (2023). Heated kaolinite-La (III) hydroxide complex for effective removal of phosphate from eutrophic water. *Applied Clay Science*, 231, 106729.

Publisher's Note Springer Nature remains neutral with regard to jurisdictional claims in published maps and institutional affiliations.

Springer Nature or its licensor (e.g. a society or other partner) holds exclusive rights to this article under a publishing agreement with the author(s) or other rightsholder(s); author self-archiving of the accepted manuscript version of this article is solely governed by the terms of such publishing agreement and applicable law.